An Amplitude- and Rate-Saturated Collective Pitch Controller for Wind Turbine Systems

Nehal Baiomy[a], Ryo Kikuuwe[b,*]

[a]*Department of Electrical Power and Machines, Cairo University, Giza, Egypt (E-mail: eng.nehal90@gmail.com)*
[b]*Department of Mechanical Systems Engineering, Hiroshima University, Hiroshima 739-8527, Japan (E-mail: kikuuwe@ieee.org)*

Abstract

This paper proposes a new collective pitch controller for wind turbine systems to maintain the generator speed constant at the rated value in the region above the rated wind speed. It provides the command of the collective pitch angle to the wind turbine system, and one can impose explicit limits on the magnitude and the rate-of-change of the pitch angle command. In addition, the controller involves a variable gain that realizes non-overshooting convergence from the large errors in the generator speed and accurate regulation of the generator speed near the rated value. This controller is an extension of an amplitude- and rate-saturated controller previously proposed by the authors. It is combined with a state and disturbance observer and a lookup table-based feedforward. The proposed controller is validated through a software simulator FAST emulating a three-bladed horizontal-axis wind turbine system.

Keywords: Actuator constraints, collective pitch control, implicit discretization, rate limitation, sliding mode, wind turbine

1. Introduction

Each variable-speed wind turbine has a rated wind speed above which a designed rated power of the turbine is achieved. The relation between the wind

*Corresponding author

speed and the generated power, which increases as the generator speed increases, of wind turbines can be illustrated as in Fig. 1. In the region called "Region 3," in which the wind speed is above the rated value, the generator speed needs to be maintained constant at the rated speed to avoid overloading on the generator [1, 2]. The regulation of the generator speed is performed by manipulating the angles of the turbine blades [2]. Each blade of them has limitations on its angle and its angle rate-of-change. The control method that would manipulate the blades' angles should be robust enough to regulate the generator speed under a wide range of wind speeds [3]. In addition, the control method should respect the limitations of the blade angle to avoid degradation in the turbine performance.

A control scheme that sends identical pitch angle commands to all blades of a turbine is referred to as collective pitch control (CPC). Various CPC methods have been developed to achieve the regulation of the generator speed in Region 3. Gain-scheduling proportional-integral controller [4, 5] is a conventional controller used with most commercial wind turbines [1]. This conventional control methodology poses difficulty in tuning the controller parameters for a wide range of wind speeds, which continuously change during operation. Disturbance accommodation control is another control methodology, which is applied ear-

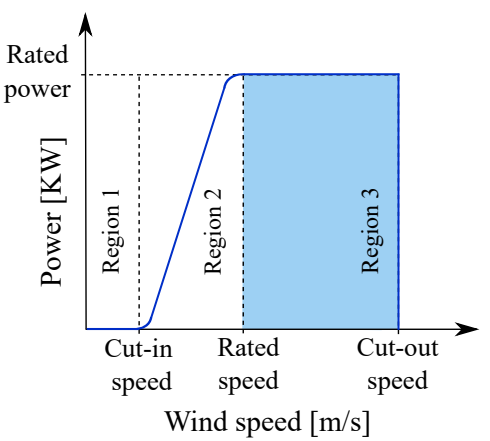

Figure 1: Relation between the wind speed and the generated power of variable-speed wind turbines.

lier to wind turbine systems [6, 7] to attenuate the effect of wind disturbances. One of its drawbacks is the sensitivity against the unmodeled dynamics of the turbine, which may cause instability in the turbine performance [8].

Some sliding mode control schemes have been proposed [9, 10, 11] to cope with the turbine structure nonlinearity and uncertainty. Beltran *et al.* [10] introduced a dynamic sliding mode controller to maintain the generated speed via controlling the torque of the generator. Their sliding mode controller employs an adaptive gain that continuously increases as long as there exists an error between the reference and the actual power of the turbine. The methodology of employing an adaptive gain proportional to the error may be undesirable for controlling the pitch angles of the turbine because, in such a case, the control signal may increase over the limitations of the pitch angles.

In order to circumvent the so-called chattering problem produced by sliding mode controllers, modified schemes have been developed, in which the sign function is relaxed into a saturation function [9, 10], while in another work, higher-order sliding mode schemes [12] are introduced. Colombo *et al.* [13] have proposed a sliding mode approach to maintain the generator speed via controlling the pitch angle, and they employed the boundary-layer method to reduce the chattering phenomenon. Although their scheme is designed to deal with several uncertainties in the model, it does not take the amplitude- and rate-limitations of the blade angle into account. As far as the authors are aware, there have been no studies employing sliding mode controllers taking into account the limitations on the blade angles and their rate-of-change.

This paper proposes a new CPC scheme with which the user can impose explicit limits on the magnitude of the pitch angle command and its rate-of-change. The new scheme is based on our previously proposed sliding mode-like controller [14]. With features inherited from the previous controller [14], the proposed CPC scheme can be set to operate within the hardware limitations of the pitch actuators. In most previous studies, hardware limitations are treated as parameter optimization problems [15, 16] or by directly imposing appropriate limiters on the controller outputs [4, 17, 18]. In contrast, the proposed

controller explicitly includes the limiters as an embedded part of a sliding mode framework. The proposed scheme involves a nonlinear function that changes the control gain according to the state and the magnitude of the disturbance. This nonlinear function facilitates a broader region of attraction when there are significant variations in the wind speed and also facilitates accurate regulation of the generator speed when the variations are small. The chattering is eliminated by a model-based implicit method [19, 20] employed in the discrete-time implementation of the controller.

The proposed controller is based on a standardized linearization scheme for the inherently nonlinear wind turbine dynamics, which is provided by a well-established wind turbine simulator, FAST ("Fatigue, Aerodynamics, Structures, and Turbulence") [21]. The validation of the proposed controller is shown through a comparative simulation study with two conventional control methods, which are a gain-scheduling proportional-integral controller [4], and a linear state-feedback controller of which the gains are obtained based on an H_2/H_∞ criteria [15].

The rest of this paper is organized as follows. Section 2 presents a reduced linear time-invariant model of the wind turbine system. Section 3 proposes the controller combined with a state and disturbance observer. Section 4 shows simulation results, including comparison with other previous methods. Section 5 provides concluding remarks of this paper.

2. Problem Formulation

We here employ the modeling scheme adopted by FAST [21], in which the wind turbine is described by the following nonlinear equation of motion:

$$\boldsymbol{M}(\boldsymbol{Q}, \boldsymbol{U}, t)\ddot{\boldsymbol{Q}} + \boldsymbol{F}(\boldsymbol{Q}, \dot{\boldsymbol{Q}}, \boldsymbol{U}, \boldsymbol{\Xi}, t) = \boldsymbol{0} \tag{1}$$

where $\boldsymbol{M}$ denotes the inertia matrix, $\boldsymbol{F}$ is a nonlinear function, and t is the time. The vector $\boldsymbol{Q}$ represents the displacements of the system's degrees of freedoms (DOFs) including the azimuth angle, the displacements of elastic components

such as the blades, the generator shaft, the drivetrain gearbox, and the tower. For a three-bladed horizontal-axis wind turbine, the full dimension of $\boldsymbol{Q}$ can be set as 24 as accounted in [21], and in such a case, we have $\boldsymbol{M} \in \mathbb{R}^{24\times 24}$ and $\boldsymbol{F} \in \mathbb{R}^{24}$. The vector $\boldsymbol{U}$ is the input to the plant, which may include the pitch angles of the blades, the nacelle yaw angle rate, and the electrical torque of the generator. The vector $\boldsymbol{\Xi}$ includes disturbances, such as the hub-height wind speed and the wind share. Throughout this paper, bold-face symbols denote vectors and matrices.

2.1. Reduced LTI Model for Controller Development

To consider a controller for the plant (1), a linear time-invariant (LTI) approximation of (1) is needed. We follow the modeling scheme adopted by FAST [21] to derive such an approximation. Considering the nature of wind turbine systems, we can see that the time dependency of the system (1) is very small. Moreover, among the many DOFs of the whole system, the rotating motions of the generator and the torsional motion of the drivetrain can be seen as two of the dominant DOFs. The drivetrain here represents the gears and other flexible components that transmit the mechanical power from the rotor shaft to the generator shaft. Thus, we can say that the dominant elements of the vector $\boldsymbol{Q}$ are θ and ϕ, which respectively denote the rotor-shaft angle (rad) and the drivetrain torsional displacement (rad). In addition, we assume that the identical pitch angle commands are sent to all blades, and thus the dominant element of $\boldsymbol{U}$ is only one command $\widehat{u} \in \mathbb{R}$, which is referred to as the collective pitch angle (rad). The dominant member of the disturbance vector $\boldsymbol{\Xi}$ is assumed to be the horizontal wind speed $\widehat{\xi} \in \mathbb{R}$ measured in m/s. Then, we can write the reduced time-invariant nonlinear model as follows:

$$\begin{bmatrix} \dot{\theta} \\ \dot{\phi} \end{bmatrix} = \begin{bmatrix} \omega \\ \nu \end{bmatrix} \tag{2}$$

$$\begin{bmatrix} \dot{\omega} \\ \dot{\nu} \end{bmatrix} = \boldsymbol{f}\left(\begin{bmatrix} \theta \\ \phi \end{bmatrix}, \begin{bmatrix} \omega \\ \nu \end{bmatrix}, \begin{bmatrix} \widehat{u} \\ \widehat{\xi} \end{bmatrix} \right) \tag{3}$$

where ω and ν are the angular velocity (rad/s) of the rotor shaft and the rate-of-change (rad/s) of the drivetrain torsion, respectively. Such a reduced-dimensional model can be obtained by FAST [21] by "disabling" specified DOFs and specifying necessary elements of $\boldsymbol{U}$ and $\boldsymbol{\Xi}$.

Here we set the following assumption:

Assumption 1. *With a given angular velocity ω_r of the rotor shaft and a given wind speed $\widehat{\xi}_m$, there exists a collective pitch angle $\widehat{u} = \widehat{u}_f(\widehat{\xi}_m, \omega_r)$ with which the system is in the steady state.*

The steady state here stands for the situation where ω is constant (at a value ω_r) and ν and ϕ exhibit cyclic behaviors of which each cycle corresponds to the rotation of θ from 0 to 2π. Actually, FAST [21] has a function to find such a steady state and the value $\widehat{u}_f(\widehat{\xi}_m, \omega_r)$ according to given values of $\widehat{\xi}_m$ and ω_r. In such a situation, $\dot{\omega} = 0$ is satisfied and ϕ, ν and $\dot{\nu}$ are functions of θ. That is, there exist appropriate functions ϕ_f, ν_f and ν_{Df} (where the subscript f stands for a function) with which the following equation is satisfied for all $\theta_0 \in [0, 2\pi)$:

$$\begin{bmatrix} 0 \\ \nu_{Df}(\theta_0, \widehat{\xi}_m, \omega_r) \end{bmatrix} = \boldsymbol{f}\left(\begin{bmatrix} \theta_0 \\ \phi_f(\theta_0, \widehat{\xi}_m, \omega_r) \end{bmatrix}, \begin{bmatrix} \omega_r \\ \nu_f(\theta_0, \widehat{\xi}_m, \omega_r) \end{bmatrix}, \begin{bmatrix} \widehat{u}_f(\widehat{\xi}_m, \omega_r) \\ \widehat{\xi}_m \end{bmatrix} \right). \tag{4}$$

Such a situation can be referred to as an "operating point," which can be defined as follows:

$$\begin{aligned} \mathcal{P}(\theta_0, \widehat{\xi}_m, \omega_r) = \ \big\{ & \theta = \theta_0,\ \phi = \phi_f(\theta_0, \widehat{\xi}_m, \omega_r),\ \omega = \omega_r,\ \nu = \nu_f(\theta_0, \widehat{\xi}_m, \omega_r), \\ & \dot{\omega} = 0,\ \dot{\nu} = \nu_{Df}(\theta_0, \widehat{\xi}_m, \omega_r),\ \ \widehat{\xi} = \widehat{\xi}_m,\ \widehat{u} = \widehat{u}_f(\widehat{\xi}_m, \omega_r) \big\}. \end{aligned} \tag{5}$$

Around an operating point $\mathcal{P}(\theta_0, \widehat{\xi}_m, \omega_r)$, one can obtain a linear approxi-

mation of the system (3) as follows:

$$\begin{bmatrix} \dot{\theta} - \omega_r \\ \dot{\phi} - \nu_f(\theta_0, \widehat{\xi}_m, \omega_r) \\ \dot{\omega} \\ \dot{\nu} - \nu_{Df}(\theta, \widehat{\xi}_m, \omega_r) \end{bmatrix} = \widehat{\boldsymbol{A}}(\theta_0, \widehat{\xi}_m, \omega_r) \begin{bmatrix} \theta - \theta_0 \\ \phi - \phi_f(\theta_0, \widehat{\xi}_m, \omega_r) \\ \omega - \omega_r \\ \nu - \nu_f(\theta_0, \widehat{\xi}_m, \omega_r) \end{bmatrix} + \widehat{\boldsymbol{B}}(\theta_0, \widehat{\xi}_m, \omega_r) \begin{bmatrix} \widehat{u} - \widehat{u}_f(\widehat{\xi}_m, \omega_r) \\ \widehat{\xi} - \widehat{\xi}_m \end{bmatrix} \tag{6}$$

where

$$\widehat{\boldsymbol{A}}(\theta_0, \widehat{\xi}_m, \omega_r) \triangleq \left[\begin{array}{cc} \boldsymbol{O}_{2\times 2} & \boldsymbol{I}_2 \\ \partial \boldsymbol{f}/\partial[\theta, \phi]^T & \partial \boldsymbol{f}/\partial[\omega, \nu]^T \end{array} \right] \Bigg|_{\mathcal{P}(\theta_0, \widehat{\xi}_m, \omega_r)} \in \mathbb{R}^{4\times 4} \tag{7}$$

$$\widehat{\boldsymbol{B}}(\theta_0, \widehat{\xi}_m, \omega_r) \triangleq \left[\begin{array}{c} \boldsymbol{O}_{2\times 2} \\ \partial \boldsymbol{f}/\partial[\widehat{u}, \widehat{\xi}]^T \end{array} \right] \Bigg|_{\mathcal{P}(\theta_0, \widehat{\xi}_m, \omega_r)} \in \mathbb{R}^{4\times 2}. \tag{8}$$

Because of the cyclic nature of the behavior and the fact that θ is not of interest for control purposes, one can consider an *averaged* dynamics of the system over $\theta_0 \in [0, 2\pi)$. Let N be a natural number. Averaging over N operating points yields the following:

$$\boldsymbol{A}(\widehat{\xi}_m, \omega_r) \triangleq \frac{1}{N} \sum_{i=1}^{N} \boldsymbol{J} \widehat{\boldsymbol{A}}(2\pi i/N, \widehat{\xi}_m, \omega_r) \boldsymbol{J}^T \in \mathbb{R}^{3\times 3} \tag{9}$$

$$\boldsymbol{B}(\widehat{\xi}_m, \omega_r) \triangleq \frac{1}{N} \sum_{i=1}^{N} \boldsymbol{J} \widehat{\boldsymbol{B}}(2\pi i/N, \widehat{\xi}_m, \omega_r) \in \mathbb{R}^{3\times 2} \tag{10}$$

$$\bar{\phi}_f(\widehat{\xi}_m, \omega_r) \triangleq \frac{1}{N} \sum_{i=1}^{N} \phi_f(2\pi i/N, \widehat{\xi}_m, \omega_r) \in \mathbb{R}. \tag{11}$$

Here, $\boldsymbol{J} \triangleq [\boldsymbol{o}_3, \boldsymbol{I}_3] \in \mathbb{R}^{3\times 4}$ where $\boldsymbol{o}_3$ is the three dimensional zero column vector, and $\boldsymbol{I}_3$ is the three dimensional identity matrix. In addition, the cyclic change of ϕ results in the following:

$$\frac{1}{N} \sum_{i=1}^{N} \nu_f(2\pi i/N, \widehat{\xi}_m, \omega_r) \approx 0 \tag{12}$$

$$\frac{1}{N} \sum_{i=1}^{N} \nu_{Df}(2\pi i/N, \widehat{\xi}_m, \omega_r) \approx 0. \tag{13}$$

As a result, we can obtain the following reduced linearized system:

$$\begin{bmatrix} \dot{\phi} \\ \dot{\omega} \\ \dot{\nu} \end{bmatrix} = \boldsymbol{A}(\widehat{\xi}_m, \omega_r) \begin{bmatrix} \phi - \bar{\phi}_f(\widehat{\xi}_m, \omega_r) \\ \omega - \omega_r \\ \nu \end{bmatrix} + \boldsymbol{B}(\widehat{\xi}_m, \omega_r) \begin{bmatrix} \widehat{u} - \widehat{u}_f(\widehat{\xi}_m, \omega_r) \\ \widehat{\xi} - \widehat{\xi}_m \end{bmatrix}. \quad (14)$$

The linearized model (14) depends on the choice of the values $\widehat{\xi}_m$ and ω_r. One reasonable choice for ω_r is the rated speed of the rotor shaft, to which the rotor shaft speed ω should be regulated by the controller to be constructed. As for the value $\widehat{\xi}_m$, a reasonable choice is the measured wind speed, which can be obtained by an appropriate sensor such as LiDAR [4] and a cup anemometer. This measured wind speed $\widehat{\xi}_m$ may be different from the true wind speed $\widehat{\xi}$, which cannot be assumed to be exactly available. One inconvenience in the use of (14) is that the matrices $\boldsymbol{A}(\widehat{\xi}_m, \omega_r)$ and $\boldsymbol{B}(\widehat{\xi}_m, \omega_r)$ vary along the time depending on the measurement $\widehat{\xi}_m$. To circumvent this inconvenience, we set a fixed value of the wind speed $\widehat{\xi}_r$ that should be chosen in the middle of the supposed range of the wind speeds, i.e., Region 3. With these fixed values ω_r and $\widehat{\xi}_r$, we set the following assumption:

Assumption 2. *The changes in $\boldsymbol{A}(\widehat{\xi}, \omega_r)$ and $\boldsymbol{B}(\widehat{\xi}, \omega_r)$ according to the change in $\widehat{\xi}$ are sufficiently small within a certain range of $\widehat{\xi}$ including $\widehat{\xi}_r$ and $\widehat{\xi}_m$.*

This assumption leads to the following approximation of (14):

$$\begin{bmatrix} \dot{\phi} \\ \dot{\omega} \\ \dot{\nu} \end{bmatrix} = \boldsymbol{A}(\widehat{\xi}_r, \omega_r) \begin{bmatrix} \phi - \bar{\phi}_f(\widehat{\xi}_m, \omega_r) \\ \omega - \omega_r \\ \nu \end{bmatrix} + \boldsymbol{B}(\widehat{\xi}_r, \omega_r) \begin{bmatrix} \widehat{u} - \widehat{u}_f(\widehat{\xi}_m, \omega_r) \\ \widehat{\xi} - \widehat{\xi}_m \end{bmatrix}. \quad (15)$$

With the fixed $\widehat{\xi}_r$ and ω_r and the measured $\widehat{\xi}_m$, let us define the following

variables:

$$\boldsymbol{x} \triangleq \begin{bmatrix} \phi - \bar{\phi}_f(\widehat{\xi}_m, \omega_r) \\ \omega - \omega_r \\ \nu \end{bmatrix} \tag{16}$$

$$u \triangleq \widehat{u} - \widehat{u}_f(\widehat{\xi}_m, \omega_r) \tag{17}$$

$$\xi \triangleq \widehat{\xi} - \widehat{\xi}_m \tag{18}$$

$$\boldsymbol{A} \triangleq \boldsymbol{A}(\widehat{\xi}_r, \omega_r) \tag{19}$$

$$[\boldsymbol{b}, \boldsymbol{g}] \triangleq \boldsymbol{B}(\widehat{\xi}_r, \omega_r). \tag{20}$$

Then, (15) is now rewritten as the following LTI system:

$$\dot{\boldsymbol{x}} = \boldsymbol{A}\boldsymbol{x} + \boldsymbol{b}u + \boldsymbol{g}\xi. \tag{21}$$

Such an LTI model, more specifically, the set of matrices $\boldsymbol{A} \in \mathbb{R}^{3\times3}$, $\boldsymbol{b} \in \mathbb{R}^3$ and $\boldsymbol{g} \in \mathbb{R}^3$, can be obtained by utilizing built-in functions of FAST [21]. Linear approximations of the form (21) of wind turbine systems have also been used by some previous researchers [15, 22].

In the LTI model (21), the state vector $\boldsymbol{x}$ is not available, except the second element being obtained through the rotor tachometer, but the later Section 3.2 will introduce a state and disturbance observer to estimate it. As for the first element of $\boldsymbol{x}$, its value is directly obtained through the observer, although ϕ is not available and $\bar{\phi}_f(\widehat{\xi}_m, \omega_r)$ does not have to be computed. Although $\widehat{\xi}_m$ is available, the true wind speed $\widehat{\xi}$ is unavailable and the measurement error ξ is to be also estimated through the observer. The control input u is to be provided by the controller to be constructed based on the LTI model (21). The actual control input $\widehat{u}$ to be given to the plant should be obtained as $\widehat{u} = u + \widehat{u}_f(\widehat{\xi}_m, \omega_r)$ as can be seen in (17). One practical solution to obtain $\widehat{u}_f(\widehat{\xi}_m, \omega_r)$ is to construct a lookup table in advance using some modeling software such as FAST [21], which would be computationally more efficient than the realtime computation.

The output equation of the LTI model (21) is as follows:

$$\Delta\omega_g = \boldsymbol{h}^T\boldsymbol{x} \tag{22}$$

where

$$\Delta\omega_g \triangleq \omega_g - \omega_{gr} \tag{23}$$

and ω_g (rpm) and ω_{gr} (rpm) are the observed and the reference generator speeds. The vector $\boldsymbol{h}$ is defined as $\boldsymbol{h} = [0, h_1, 0]^T$ where h_1 is the product of the gear ratio and the conversion coefficient from rad/s to rpm (i.e., $h_1 = \omega_{gr}$ (rpm)$/\omega_r$ (rad/s)).

Remark 1. *It should be noted that the LTI model (21) is an approximation of the nonlinear system (1) neglecting the motions of 22 DOFs, and it does not even include any error terms that may be caused by this approximation. The simulation software package FAST [21] actually has well-established built-in functions to provide the LTI approximation (21) with given values of $\widehat{\xi}_r$ and ω_r. Our controller developed in Section 3 will be built upon this simplified LTI model (21), but the validation of the controller will be performed with the fully nonlinear time-variant plant (1) in the simulations in Section 4.*

2.2. Pitch Actuator Limitations

Each blade of the wind turbine has a pitch actuator that receives the control signal $\widehat{u}$ and changes the blade angle accordingly around its longitudinal axis. Due to its intrinsic mechanical properties, the angle and the angular velocity of the blades are limited. That is, the control signal $\widehat{u}$ needs to satisfy the following conditions:

$$|\widehat{u}| \leq \alpha, \qquad |d\widehat{u}/dt| \leq \beta \tag{24}$$

where α and β are positive constants. For example, the pitch actuators of a 5-MW wind turbine discussed in [4] have the limits $\alpha = 1.5$ rad and $\beta = 0.14$ rad/s.

3. Colletive Pitch Controller

3.1. Extension of Amplitude- and Rate-Saturated Controller

This section extends our previous controller [14], which we call an amplitude- and rate-saturated controller, to be able to deal with wind turbine systems.

Because the previous controller [14] was developed for a class of LTI systems, we use the LTI approximation (21) of the wind-turbine dynamics (1) as the basis for the controller design.

The controller to be constructed in this section intends to impose specified limits on $|u|$ and $|\dot{u}|$, where u is the control input of the LTI approximation (21). Meanwhile, the hardware limits α and β, which appear in (24), restrict the actual control command $\widehat{u} = u + \widehat{u}_f(\widehat{\xi}_m, \omega_r)$, instead of only the u component. One way to comply with the hardware limits α and β is to impose fixed limits to each of the components u and $\widehat{u}_f(\widehat{\xi}_m, \omega_r)$, i.e., to set fixed values $\alpha_u \in (0, \alpha)$ and $\beta_u \in (0, \beta)$ with which the followings should be satisfied:

$$|u| \le \alpha_u \ , \quad |\dot{u}| \le \beta_u, \tag{25}$$

$$|\widehat{u}_f(\widehat{\xi}_m, \omega_r)| \le \alpha - \alpha_u \ , \quad \left| \frac{d\widehat{u}_f(\widehat{\xi}_m, \omega_r)}{dt} \right| \le \beta - \beta_u. \tag{26}$$

Imposing fixed limits to each component is for the simplicity of implementation, and it may be too conservative especially when either of them is unexpectedly small. An imaginable workaround is to set α_u and β_u adaptively according to $\widehat{u}_f(\widehat{\xi}_m, \omega_r)$ and its rate-of-change, but such sophistication is left for future study.

By adapting the main part of our previous controller [14] to the plant (21) with the input constraints (25), one obtains a controller of the following form:

$$\dot{u} \in -\beta_u \mathrm{sgn}\left(u + \mathrm{sat}_{\alpha_u}(\boldsymbol{c}^T \boldsymbol{x}/\gamma(\boldsymbol{x}, u))\right) \tag{27}$$

where the vector $\boldsymbol{c} \in \mathbb{R}^3$ is a controller parameter that should be chosen appropriately and $\gamma(\boldsymbol{x}, u)$ is a nonlinear function defined later. The sgn and sat functions are defined as follows:

$$\mathrm{sgn}(x) \triangleq \begin{cases} [-1, 1] & \text{if } x = 0 \\ x/|x| & \text{if } x \neq 0, \end{cases} \tag{28}$$

$$\mathrm{sat}_\alpha(x) \triangleq \begin{cases} x & \text{if } |x| \le \alpha \\ \alpha x/|x| & \text{if } |x| > \alpha. \end{cases} \tag{29}$$

With the expanded system composed of the LTI plant (21) and the controller (27), the state vector can be defined as $[\boldsymbol{x}^T, u]^T$. In the state space of this

expanded system, the equation

$$u + \mathrm{sat}_{\alpha_u}(\boldsymbol{c}^T\boldsymbol{x}/\gamma) = 0 \tag{30}$$

represents the switching surface of the controller (27). With γ being fixed, in the same way as in the proof of [14, Theorem 1], it is straightforward to prove that

$$\frac{d}{dt}\left|u + \mathrm{sat}_{\alpha_u}(\boldsymbol{c}^T\boldsymbol{x}/\gamma)\right| < 0 \tag{31}$$

is satisfied as long as

$$\frac{|\boldsymbol{c}^T\boldsymbol{A}\boldsymbol{x} + \boldsymbol{c}^T\boldsymbol{b}u + \boldsymbol{c}^T\boldsymbol{g}\xi|}{\beta_u} < \gamma \tag{32}$$

is satisfied. It implies that the sliding mode takes place in the subset of the switching surface (30) in which (32) is satisfied. When the system is in the sliding mode on the linear portion of the switching surface (30), i.e., the subset of (30) where $|\boldsymbol{c}^T\boldsymbol{x}/\gamma| < \alpha_u$, the controller (27) reduces to a linear controller $u = -\boldsymbol{c}^T\boldsymbol{x}/\gamma$. In this case, a smaller value of γ facilitates a high-gain control action that attracts the state to a smaller neighborhood of the origin [14], mitigating the influence of disturbances. Meanwhile, (32) implies that a larger value of γ results in a larger region in which the sliding mode may take place, as well as a larger region of attraction, as discussed in [14, Section III]. In addition, in the sliding mode, the behavior of the system near the origin is determined by the eigenvalues of the matrix $\boldsymbol{A} - \boldsymbol{b}\boldsymbol{c}^T/\gamma$, of which the Hurwitzness is a necessary condition of the asymptotic stability of the origin.

Our previous paper [14] employed a particular definition of the nonlinear function $\gamma(\boldsymbol{x}, u)$ to enlarge the region of attraction when the state is far from the origin and to shrink the terminal attractor when the state is near the origin. Because the plant (21) in this paper is slightly different from the plant in the previous paper [14], this paper proposes a slightly modified definition of $\gamma(\boldsymbol{x}, u)$, which is described as follows:

$$\gamma(\boldsymbol{x}, u) \triangleq \min\left(\gamma_c, \frac{|\boldsymbol{c}^T\boldsymbol{A}\boldsymbol{x}| + \boldsymbol{c}^T\boldsymbol{b}|u| + |\boldsymbol{c}^T\boldsymbol{g}\xi| + \boldsymbol{c}^T\boldsymbol{b}L}{\beta_u}\right) \tag{33}$$

where γ_c and L are positive scalars that need to be appropriately chosen. Here, $\boldsymbol{c}^T\boldsymbol{b} > 0$ is assumed to be satisfied, and one can see that $\gamma(\boldsymbol{x}, u)$ varies within the interval $[\gamma_{\min}, \gamma_c]$ where $\gamma_{\min} \triangleq \boldsymbol{c}^T\boldsymbol{b}L/\beta_u > 0$. This definition of $\gamma(\boldsymbol{x}, u)$ is inspired by the condition (32), which is satisfied as long as $\gamma(\boldsymbol{x}, u) < \gamma_c$. The parameter γ_c should be large enough to assure a sufficiently large region of attraction but should not be too large to hold the eigenvalues of the matrix $\boldsymbol{A} - \boldsymbol{b}\boldsymbol{c}^T/\gamma(\boldsymbol{x}, u)$ inside a given subset of the left half of the complex plane. The value of the parameter L, which is proportional to $\gamma_{\min}$, should be chosen small enough to realize a sufficiently small terminal attractor. We at this time do not have a clear guideline for the choice of L, although our previous paper [14] suggested a guideline depending on the upperbound of the disturbance superposed to the input u, which is absent in the plant (21).

Remark 2. *The previous paper [14] has presented some stability analysis on a controller of the form (27) combined with a linear plant. The analysis is only on the reachability to the sliding mode and the local stability near the origin on the sliding surface, and it does not consider the effect of the temporal change in γ. The new controller depends on the analysis in the previous paper, but the limitations in theoretical aspects remain. Leaving theoretical investigation as future work, this paper focuses on the extension of the controller toward a real-world application, i.e., wind turbine systems, and its empirical validation through realistic simulation setup, i.e., FAST.*

In applications to wind-turbine systems, the proposed controller (27) combined with (33) needs to be implemented to discrete-time digital devices. We need to avoid the chattering caused by inappropriate treatment of the set-valued sgn function in the discretization of (27). Our previous paper [14] employed a model-based implicit discretization scheme [19, 20] to obtain a discrete-time algorithm of the controller. In the same light, we propose the following discrete-

time algorithm as an implementation of the controller (27) combined with (33):

$$w_{k-1} := \boldsymbol{c}^T(\boldsymbol{I} + h\boldsymbol{A})\boldsymbol{x}_{k-1} \tag{34a}$$

$$\gamma_k := \min\left(\gamma_c, \frac{|\boldsymbol{c}^T\boldsymbol{A}\boldsymbol{x}_{k-1}| + \boldsymbol{c}^T\boldsymbol{b}|u_{k-1}| + |\boldsymbol{c}^T\boldsymbol{g}\xi_{k-1}| + \boldsymbol{c}^T\boldsymbol{b}L}{\beta_u}\right) \tag{34b}$$

$$u_k := u_{k-1} - \mathrm{sat}_{h\beta_u}\left(u_{k-1} + \mathrm{sat}_{\alpha_u}\left(\frac{w_{k-1}}{\gamma_k + \boldsymbol{c}^T\boldsymbol{b}h}\right)\right) \tag{34c}$$

where h is the sampling interval and k is the discrete-time index.

3.2. State and Disturbance Observer

The controller (34), of which the continuous-time representation is (27) combined with (33), requires the state $\boldsymbol{x}$ and the residual disturbance ξ to be available, but they cannot be measured directly. One method to estimate them is the use of an observer called an unknown input observer (UIO) [23]. An early version of UIO was introduced by Johnson [24]. He later extended it to be a part of a disturbance accommodation controller [6], which has also been applied to wind turbine systems [7, 8].

In the same light as in [7, 25], a direct application of an UIO to the plant composed of (21) and (22) can be obtained as follows:

$$\frac{d}{dt}\begin{bmatrix} \boldsymbol{x}_e \\ \xi_e \end{bmatrix} = \boldsymbol{\mathcal{A}}\begin{bmatrix} \boldsymbol{x}_e \\ \xi_e \end{bmatrix} + \boldsymbol{\mathcal{B}}u + \boldsymbol{K}(\Delta\omega_g - \boldsymbol{h}^T\boldsymbol{x}_e) \tag{35}$$

where

$$\boldsymbol{\mathcal{A}} \triangleq \begin{bmatrix} \boldsymbol{A} & \boldsymbol{g} \\ \boldsymbol{o}_3^T & 0 \end{bmatrix}, \quad \boldsymbol{\mathcal{B}} \triangleq \begin{bmatrix} \boldsymbol{b} \\ 0 \end{bmatrix}. \tag{36}$$

Here, $\boldsymbol{x}_e \in \mathbb{R}^3$ and $\xi_e \in \mathbb{R}^3$ are estimators of the state vector $\boldsymbol{x}$ and the residual disturbance ξ, respectively. The observer gain $\boldsymbol{K} \in \mathbb{R}^4$ can calculated via a pole placement problem to locate the eigenvalues of $(\boldsymbol{\mathcal{A}} - \boldsymbol{K}\boldsymbol{\mathcal{H}})$ at desired locations, where $\boldsymbol{\mathcal{H}} = [\boldsymbol{h}^T, 0]$. This observer structure of course requires the observability of the pair $\{\boldsymbol{\mathcal{A}}, \boldsymbol{\mathcal{H}}\}$, which can be easily checked when the linearized model is obtained. At this time, we do not have a strict proof of the observability of the pair $\{\boldsymbol{\mathcal{A}}, \boldsymbol{\mathcal{H}}\}$ of wind turbine systems, but at least a wind turbine model

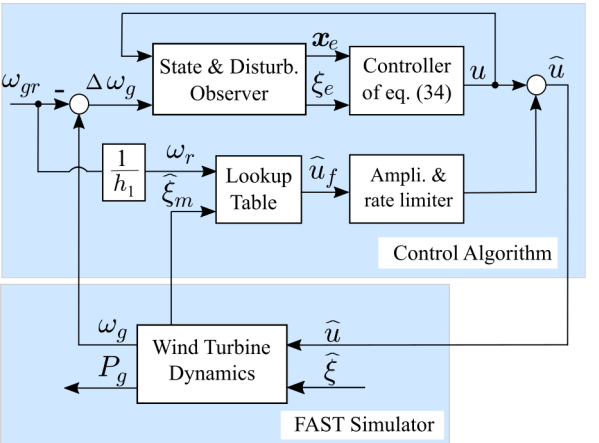

Figure 2: Block diagram of the proposed control scheme, where P_g is the generated power and $h_1 = 926.3$, which appears in (39).

provided by FAST [21] presented in the next section is indeed observable. The overall control scheme including this observer is shown in Fig. 2.

3.3. Parameter Design

To implement the discrete-time algorithm (34), we need to set the values of the parameters $\{\boldsymbol{A}, \boldsymbol{b}, \boldsymbol{g}, \alpha_u, \beta_u, L, \boldsymbol{c}, \gamma_c\}$. Among them, $\{\boldsymbol{A}, \boldsymbol{b}, \boldsymbol{g}, \alpha_u, \beta_u\}$ are determined by the physical properties of the plant (21), while the rest ones, $\{L, \boldsymbol{c}, \gamma_c\}$, need to be carefully designed. In our previous paper [26], we proposed a selection procedure for the parameters $\{\boldsymbol{c}, \gamma_c\}$, based on the assumption that L is given in advance. The procedure was based on the following two main objectives. One is to make $\|\boldsymbol{c}/\gamma_c\|$ small to enlarge the region in which the sliding mode occurs, i.e., in which the condition (32) is satisfied. The second is to keep all the eigenvalues of $\boldsymbol{A} - \boldsymbol{b}\boldsymbol{c}^T/\gamma(\boldsymbol{x}, u)$ inside a specified region $\mathcal{R}$ in the left half of the complex plane. Further discussion and details are found in [26].

Table 1: Wind Turbine Specifications [4, Table 1-1].

Power rating	5000 kW
Number of blades	3
Rotor diameter	126 m
Hub Height	90 m
Cut-in wind speed	3 m/s
Rated wind speed	11.4 m/s
Cut-out wind speed	25 m/s
Cut-in rotor speed	6.9 rpm
Rated rotor speed	12.1 rpm
Gearbox ratio	97:1
Rated generator speed	1173.7 rpm

4. Simulation Setup and Results

4.1. Simulation Setup

We conducted some simulations to validate the proposed control scheme with the wind turbine simulator FAST [21]. The simulator employed the 24-DOF nonlinear dynamics model of a 5-MW, three-bladed, variable-speed, horizontal-axis wind turbine model detailed in [4], of which the Appendices include required files to emulate the turbine by FAST. The same model has been used by some previous researchers [13, 15, 22]. Its main specifications are listed in Table 1. As illustrated in Fig. 2, the wind turbine model was connected with the control algorithm via Simulink interface. The control algorithm was composed of the proposed controller (34), the state and disturbance observer (35) and the feed-forward through the lookup table $\widehat{u}_f(\widehat{\xi}_m, \omega_r)$. The initial speed of the turbine was set to be equal to the rated speed $\omega_r = 12.1$ rpm, and the initial state of the state and disturbance observer was set as $[\boldsymbol{x}_e^T, \xi_e]^T = \boldsymbol{o}_4$.

As has been detailed in Section 3.1, the proposed controller is based on the matrices $\boldsymbol{A}$, $\boldsymbol{b}$ and $\boldsymbol{g}$ of the linear apporximation (21) of the plant. To obtain

these matrices, we used the linearization functions of FAST [21] at a particular operating point of $\mathcal{P}(\widehat{\xi}_r, \omega_r)$. Following the guideline mentioned in Section 2.1, we set $\widehat{\xi}_r = 18$ m/s, which is within Region 3, between the rated wind speed and the cut-out wind speed, and also set $\omega_r = 1.27$ rad/s, which is equivalent to the rated rotor speed 12.1 rpm. The obtained matrices were as follows:

$$\boldsymbol{A} = \begin{bmatrix} 0 & 0 & 1 \\ 172.6 & -2.731 & 1.237 \\ -195 & 2.4555 & -1.6725 \end{bmatrix}, \tag{37}$$

$$\boldsymbol{b} = \begin{bmatrix} 0 \\ 0 \\ -1.3265 \end{bmatrix}, \ \boldsymbol{g} = \begin{bmatrix} 0 \\ 0 \\ 0.0308 \end{bmatrix}, \tag{38}$$

$$\boldsymbol{h} = \begin{bmatrix} 0 & 926.3 & 0 \end{bmatrix}^T. \tag{39}$$

The second element of $\boldsymbol{h}$ is the ratio between the generator speed in rpm and the rotor-shaft speed in rad/s, which is the reduction ratio 97 of the gearbox multiplied by $60/(2\pi)$. The hardware limits on the control input $\widehat{u}$ were set as $\alpha = 1.5$ rad and $\beta = 0.14$ rad/s as suggested in [4], and the limits on the component u were set as $\alpha_u = 0.5$ rad and $\beta_u = 0.06$ rad/s.

We also performed the linearization process of FAST with a set of steady wind speed values $\widehat{\xi}_m$ from 12 m/s to 22 m/s to obtain the corresponding pitch angles $\widehat{u}_f(\widehat{\xi}_m, \omega_r)$. The result was obtained as a lookup table shown in Table 2. In a real implementation, the wind speed $\widehat{\xi}_m$ is supposed to be measured via proper sensors such as LiDAR [4] and a cup anemometer.

The parameters for the controller (34) were chosen as $L = 0.05$, $\gamma_c = \infty$ and $\boldsymbol{c} = [-0.2130, -0.0225, -0.0081]^T$, partially through the procedure presented in [26]. We needed some trial and error for the parameter tuning because the procedure in [26] were originally for the plant defined in [14], which is slightly different from the plant (21) of the present paper. Specifically, we initially set the parameter L to be $L = 0.001$ and performed the procedure to obtain $\boldsymbol{c}$ and γ_c. After that, by observing our preliminary simulation results, we tuned L manually and ended up with $L = 0.05$. In the application of the procedure

Table 2: The Lookup table of $\widehat{u}_f(\widehat{\xi}_m, \omega_r)$ with $\omega_r = 1.27$ rad/s.

$\widehat{\xi}_m$	$\widehat{u}_f(\widehat{\xi}_m, \omega_r)$
12 m/s	0.077266 rad
13 m/s	0.121026 rad
14 m/s	0.155668 rad
15 m/s	0.185741 rad
16 m/s	0.213168 rad
17 m/s	0.238465 rad
18 m/s	0.262362 rad
19 m/s	0.285104 rad
20 m/s	0.306746 rad
21 m/s	0.327591 rad
22 m/s	0.347891 rad

[26], auxiliary inputs were set as (cf. [26] for definitions): $R = 1$, $\boldsymbol{Q} = 10^{-4}\boldsymbol{I}$, $\delta_1 \in [0.01, 1]$, $\delta_2 \in [1, 1000]$, $\gamma_{\min} \in [10^{-7}, 0.01]$, and $\mathcal{R}$ was set as the whole left half of the complex plane. We also used the matrix $\boldsymbol{T} = \mathrm{diag}[-1, -1, -0.7539]$ to transform the linearized system into the equivalent system satisfying $\boldsymbol{Tb} = [0, 0, 1]^T$, which was necessary for the procedure. As a result, we obtained the aforementioned values of $\boldsymbol{c}$ and γ_c and the auxiliary outputs $\gamma_{\min} = 1.8 \times 10^{-5}$, $\delta_1 = 0.01$, and $\delta_2 = 1000$. Fig. 3 shows the root loci of the matrix $\boldsymbol{A} - \boldsymbol{bc}^T/\gamma$ with varying γ, showing that the eigenvalues are within $\mathcal{R}$ for any $\gamma \in [\gamma_{\min}, \infty)$.

We set the sampling interval of the discrete-time implementation (34) as $h = 0.01$ s. Regarding the state and disturbance observer, we can see that the pair $\{\boldsymbol{\mathcal{A}}, \boldsymbol{\mathcal{H}}\}$ is observable from the definitions of $\boldsymbol{A}$, $\boldsymbol{g}$, and $\boldsymbol{h}$ in (37)-(39). We set the gain vector of the observer as $\boldsymbol{K} = [0.05, 0.19, 0.86, 200]^T$, with which the eigenvalues of $(\boldsymbol{\mathcal{A}} - \boldsymbol{K}\boldsymbol{\mathcal{H}})$ are placed at -10, -20, -50, and -100.

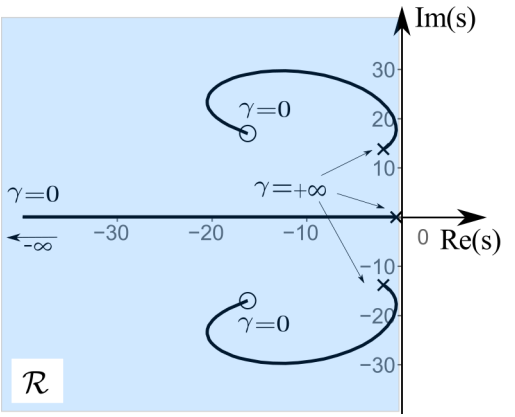

Figure 3: The loci of the eigenvalues of the matrix $(\boldsymbol{A} - \boldsymbol{b}\boldsymbol{c}^T/\gamma)$, which are within the left half of the complex plane.

4.2. Conventional Controllers for Comparison

We compare our controller with two conventional controllers. One is a gain-scheduling PI controller described in [4]. This controller employs a gain-correction factor to automatically modify the proportional and integral gains corresponding to the latest value of the collective pitch angle. Further details about the gain-correction factor can be found in [4]. Here, we set the proportional and integral gains as 0.0019 and 0.0008, respectively, and the gain-correction factor as $1/(1 + (\widehat{u}/0.11))$.

The other is the controller shown in Fig. 4, which is a linear state-feedback controller combined with a linear state observer and a feedforward term, which is represented as $\widehat{u}_f$ in the figure. This controller is motivated by the controller of Hassan *et al.* [15], who proposed an optimization method for a linear controller for wind turbines combined with some sophisticated techniques such as Kalman filtering and individual pitch control. In the controller of Fig. 4, we chose the gain vector $\boldsymbol{k}$ particularly as:

$$\boldsymbol{k} = [3.5842, 2.0471, 1.6246]^T, \tag{40}$$

which is suggested by Hassan *et al.* [15], who applied their H_2/H_∞ optimization

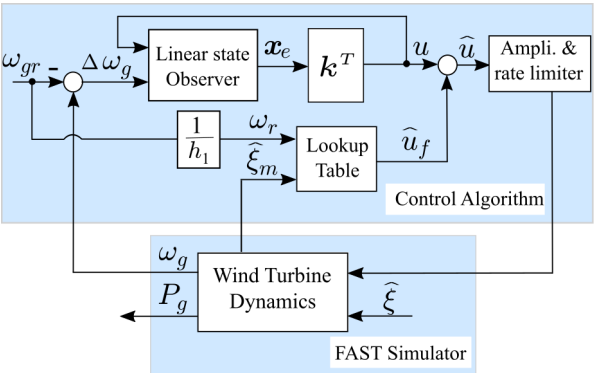

Figure 4: Block diagram of the linear feedback controller that we used in the comparison study. The vector $\boldsymbol{k}$ was chosen as in (40), which is an optimized result obtained by Hassan *et al.* [15]. Other notations are consistent with Fig. 2.

technique to the same plant as ours. As for the linear observer in Fig. 4, we chose the observer gains so that its poles were placed at $\{-10, -20, -50\}$.

Both conventional controllers include the pitch actuator limitations (24) imposed on the amplitude and the rate-of-change of the total control action $\widehat{u}$, as shown in Fig. 4.

4.3. Simulation Results

Simulations were performed with two distinctly different patterns of the wind. One was a profile of the wind speed that stochastically fluctuates and the other was the one that abruptly changes. Recall that the control objective is to maintain the generator speed ω_g and the generated power P_g at their rated values, i.e., $\omega_{gr} = 1173.7$ rpm and 5000 kW, respectively. Fig. 5 shows the results with a stochastic wind speed profile. It can be seen that, in terms of the fluctuations in the generator speed ω_g and the generated power P_g around their rated values, the gain-scheduling PI controller results in much worse performance than the other two. The linear controller and the proposed controller result in the accuracy of almost the same level as each other, although the accuracy of the proposed controller is slightly better as can be seen in Table 3.

Table 3: The mean and standard deviation of the results of the proposed and the linear controllers shown in Fig. 5, under the stochastic wind profile.

		Mean	Std. dev.
Rated values	Gen. Speed	1173.7 rpm	
	Gen. Power	5000 kW	
Proposed controller	Gen. Speed	1172 rpm	2.931 rpm
	Gen. Power	4879 kW	112.7 kW
Linear controller	Gen. Speed	1171 rpm	3.01 rpm
	Gen. Power	4867 kW	116.4 kW

With the proposed controller, Fig. 5 shows that γ maintains low values, with which high-gain control action is intended to be produced. Such high-gain actions can be observed from the jagged profile of the control signal $\widehat{u}$ and the relatively small fluctuation in the generator speed ω_g. Such features are in contrast to the smooth control signal $\widehat{u}$ and the fluctuating generator speed ω_g of the gain-scheduling PI controller, which can be seen as the results of low-gain actions.

Fig. 6 shows the results with a step-like wind profile, of which the magnitude of the variation is much larger than that in Fig. 5. At abrupt changes in the wind speed $\widehat{\xi}$, the gain-scheduling PI controller results in relatively slow convergence without overshoots, while the linear controller produces fast convergence with some overshoots and oscillation. In contrast, the proposed controller results in fast convergence with smaller overshoots and oscillation, which can be attributed to the temporal change in γ. With the proposed controller, when the wind speed abruptly changes, γ becomes larger. It results in low-gain actions, which is visible from the smaller overshoots in the generator speed ω_g. Once the wind speed settles and the generator speed ω_g approaches its rated value ω_{gr}, γ becomes smaller. It results in high-gain actions, which can be seen from the smaller fluctuation in the generator speed ω_g and the generated power P_g. Such varying actions of the proposed controller are in contrast to those of the gain-

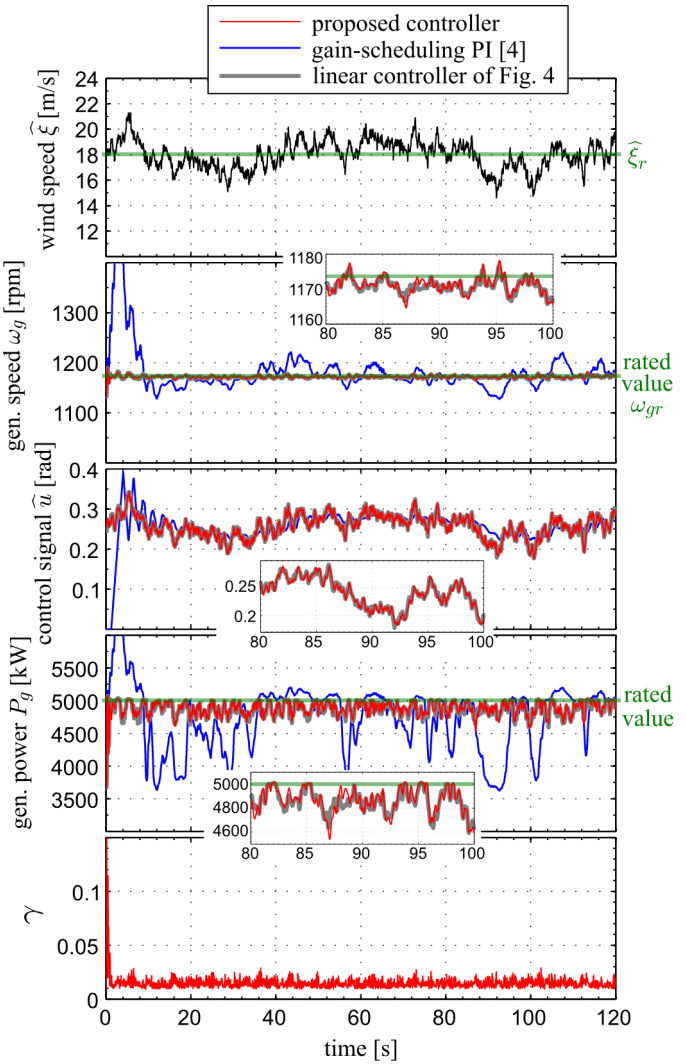

Figure 5: Simulation results with a stochastic wind speed profile of the proposed control scheme (red), the gain-scheduling PI controller (blue) [4], and the linear controller (dark gray) shown in Fig. 4.

scheduling PI controller and the linear controller, which continue producing low-gain actions and high-gain actions, respectively, for the whole simulation period.

Through Fig. 5 and Fig. 6, we can conclude that the proposed controller

is advantageous over an optimized linear controller and the gain-scheduling PI controller in that it realizes both the high tracking accuracy under relatively small wind-speed variations and the non-overshooting convergence behavior at abrupt changes in the wind speed. It should also be noted that the LTI model (21), on which the controller is based, is obtained at the wind speed $\widehat{\xi}_r$, based on Assumption 2. The results show that, even when the wind speed $\widehat{\xi}$ deviates from $\widehat{\xi}_r$, the proposed controller properly regulates the generator speed ω_g to the reference value ω_{gr}.

5. Conclusions

This paper has proposed a new collective pitch controller to maintain the generator speed at its rated value in Region 3. The proposed controller, which is an extension of the controller proposed in the authors' previous paper [14], respects the limitations of the blade angles by producing the control signal with a limited amplitude and a limited rate-of-change. The simulation results have shown that the proposed controller is robust against significant variations in wind speed.

One important feature of the technique presented in this paper is that it explicitly includes the limits of the pitch angle command and its rate-of-change in the framework of sliding mode control. Chattering is avoided with the use of the implicit discretization of the controller. High robustness of the generator performance realized by the proposed controller would be beneficial also for improving the performance of a wind farm. Since the proposed controller only manipulates the pitch angles, it would be able to be combined with appropriate yaw angle controllers [27, 28] to optimize the total performance of a wind farm.

Extending the proposed controller for MIMO systems is highly needed in a future study to consider the mechanical fatigue loads on the blades in addition to the regulation of the generator speed. Theoretical validation considering the nonlinearity of the controller and the plant, possibly employing a new Lyapunov function, is also to be addressed.

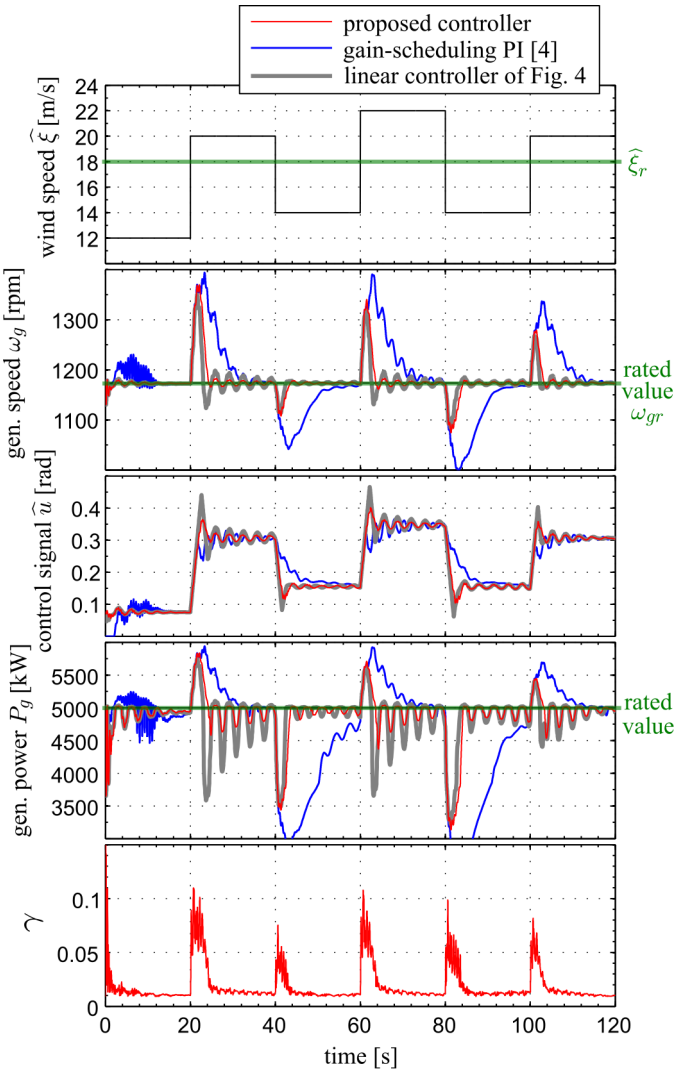

Figure 6: Simulation results with a step-like wind speed profile of the proposed control scheme (red), the gain-scheduling PI controller (blue) [4], and the linear controller (dark gray) shown in Fig. 4.

References

[1] J. G. Njiri, D. Söffker, State-of-the-art in wind turbine control: Trends and challenges, Renewable and Sustainable Energy Reviews 60 (2016) 377–393.

[2] E. Muljadi, C. P. Butterfield, Pitch-controlled variable-speed wind turbine generation, IEEE Transactions on Industry Applications 37 (1) (2001) 240–246.

[3] T. Burton, D. Sharpe, N. Jenkins, E. Bossanyi, The Controller, in Wind Energy Handbook, John Wiley & Sons, 2001, ch. 8, sec. 8.3, p. 484.

[4] J. Jonkman, S. Butterfield, W. Musial, G. Scott, Definition of a 5-MW reference wind turbine for offshore system development, Tech. Rep. NREL/TP-500-38060, National Renewable Energy Laboratory (2009).

[5] H. Takaai, Y. Chida, K. Sakurai, T. Isobe, Pitch angle control of wind turbine generator using less conservative robust control, Proceeding of IEEE Control Applications (2009) 542–547.

[6] C. D. Johnson, Theory of distrubance-accommodating controllers, Advances in Control and Dynamic Systems, 12 (1976) 387–489.

[7] M. Balas, Y. Lee, L. Kendall, Disturbance tracking control theory with application to horizontal axis wind turbines, Proceeding of the 1998 ASME Wind Energy Symposium (1998) 95–99.

[8] I. P. Girsang, J. S. Dhupia, Collective pitch control of wind turbines using stochastic disturbance accommodating control, Wind Engineering 37 (5) (2013) 517–533.

[9] S. H. Lee, Y. J. Joo, J. Back, J. H. Seo, Sliding mode controller for torque and pitch control of wind power system based on PMSG, Proceeding of International Conference on Control, Automation and Systems (2010) 1079–1084.

[10] B. Beltran, T. Ahmed-Ali, M. E. H. Benbouzid, Sliding mode power control of variable-speed wind energy conversion systems, IEEE Transactions on Energy Conversion 23 (2) (2008) 551–558.

[11] H. De Battista, R. J. Mantz, C. F. Christiansen, Dynamical sliding mode power control of wind driven induction generators, IEEE Transactions on Energy Conversion 15 (4) (2000) 451–457.

[12] B. Beltran, T. Ahmed-Ali, M. E. H. Benbouzid, High-order sliding-mode control of variable-speed wind turbines, IEEE Transactions on Industrial Electronics 56 (9) (2009) 3314–3321.

[13] L. Colombo, M. L. Corradini, G. Ippoliti, G. Orlando, Pitch angle control of a wind turbine operating above the rated wind speed: A sliding mode control approach, ISA Transactions 96 (2020) 95–102.

[14] N. Baiomy, R. Kikuuwe, An amplitude- and rate-saturated controller for linear plants, Asian Journal of Control 22 (1) (2020) 77–91.

[15] H. M. Hassan, A. L. ElShafei, W. A. Farag, M. S. Saad, A robust LMI-based pitch controller for large wind turbines, Renewable Energy 44 (2012) 63–71.

[16] M. A. Abdelbaky, X. Li, D. Jiang, Design and implementation of partial offline fuzzy model-predictive pitch controller for large-scale wind-turbines, Renewable Energy 145 (2020) 981–996.

[17] H. Badihi, Y. Zhang, H. Hong, Fuzzy gain-scheduled active fault-tolerant control of a wind turbine, Journal of Franklin Institute 351 (2013) 3677–3706.

[18] H. Zhu, M. Sueyoshi, C. Hu, S. Yoshida, A study on a floating type shrouded wind turbine: Design, modeling and analysis, Renewable Energy 134 (2019) 1099–1113.

[19] V. Acary, B. Brogliato, Implicit Euler numerical scheme and chattering-free implementation of sliding mode systems, Systems & Control Letters 59 (5) (2010) 284–293.

[20] O. Huber, V. Acary, B. Brogliato, Lyapunov stability and performance analysis of the implicit discrete sliding mode control, IEEE Transactions on Automatic Control 61 (10) (2016) 3016–3030.

[21] J. M. Jonkman, M. L. Buhl, Jr., FAST user's guide, Tech. Rep. NREL/EL-500-38230, National Renewable Energy Laboratory (2005).

[22] A. Lasheen, A. L. Elshafei, Wind-turbine collective-pitch control via a fuzzy predictive algorithm, Renewable Energy 87 (2016) 298–306.

[23] W. Chen, J. Yang, L. Guo, S. Li, Disturbance-observer-based control and related methods — An overview, IEEE Transactions on Industrial Electronics 63 (2) (2016) 1083–1095.

[24] C. D. Johnson, Optimal control of the linear regulator with constant disturbances, IEEE Transactions on Automatic Control 13 (4) (1968) 416–421.

[25] K. T. Magar, M. Balas, S. Frost, N. Li, Adaptive state feedback — Theory and application for wind turbine control, Energies 10 (12) (2017) 1–15.

[26] N. Baiomy, R. Kikuuwe, Parameter selection procedure for an amplitude- and rate-saturated controller, International Journal of Control, Automation and Systems 17 (4) (2019) 926–935.

[27] M. F. Howland, S. K. Lele, J. O. Dabiri, Wind farm power optimization through wake steering, Proceedings of the National Academy of Sciences of USA 116 (29) (2019) 14495–14500.

[28] M. Bastankhah, F. Porté-Agel, Wind farm power optimization via yaw angle control: A wind tunnel study, Journal of Renewable Sustainable Energy 11 (2019) 023301.